Supplementary Information (SI) for Materials Horizons.
This journal is © The Royal Society of Chemistry 2024

Supporting Information:

High Dense Lath Twins Upgrade High Thermoelectric Efficiency in Bi_2Te_3 Modules

Qianqian Sun[1, 2, †], Gang Wu [1, 2, †], Xiaojian Tan[1, 2, *], Qiang Zhang [1, 2, *], Zhe Guo[1], Qiaoyan Pan[1, 2], Guoqiang Liu[1, 2], Peng Sun[1], Jiehua Wu[1], Jun Jiang[1, 2, *]

[1] Ningbo Institute of Materials Technology and Engineering, Chinese Academy of Sciences, Ningbo 315201, China

[2] University of Chinese Academy of Sciences, Beijing 100049, China

*Corresponding author. E-mail: tanxiaojian@nimte.ac.cn, qiangzhang@nimte.ac.cn, jjun@nimte.ac.cn

† These authors contribute equally.

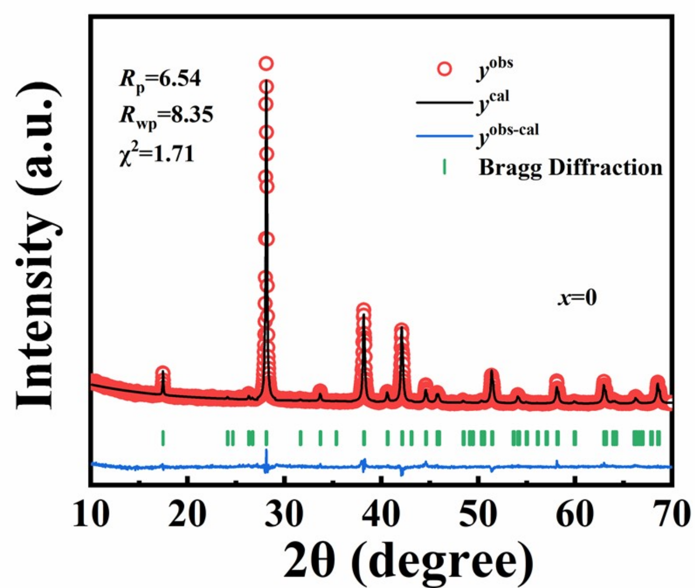

Figure S1. Rietveld refined XRD patterns of x = 0 at room temperature.

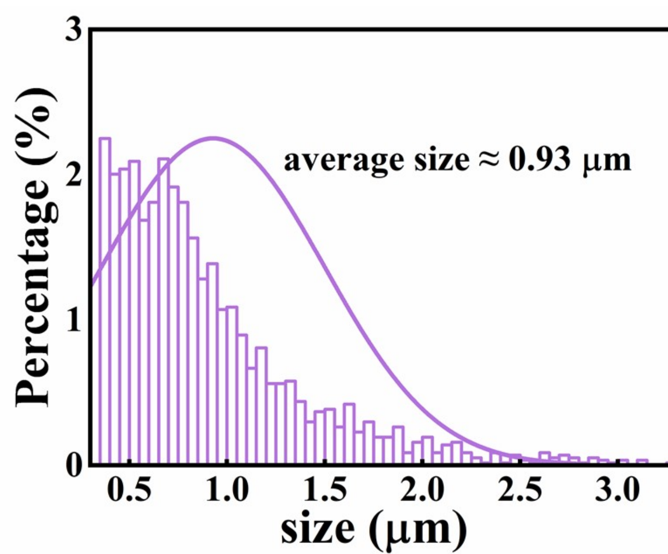

Figure S2. The distributions of crystallite size for x = 0.03 sample.

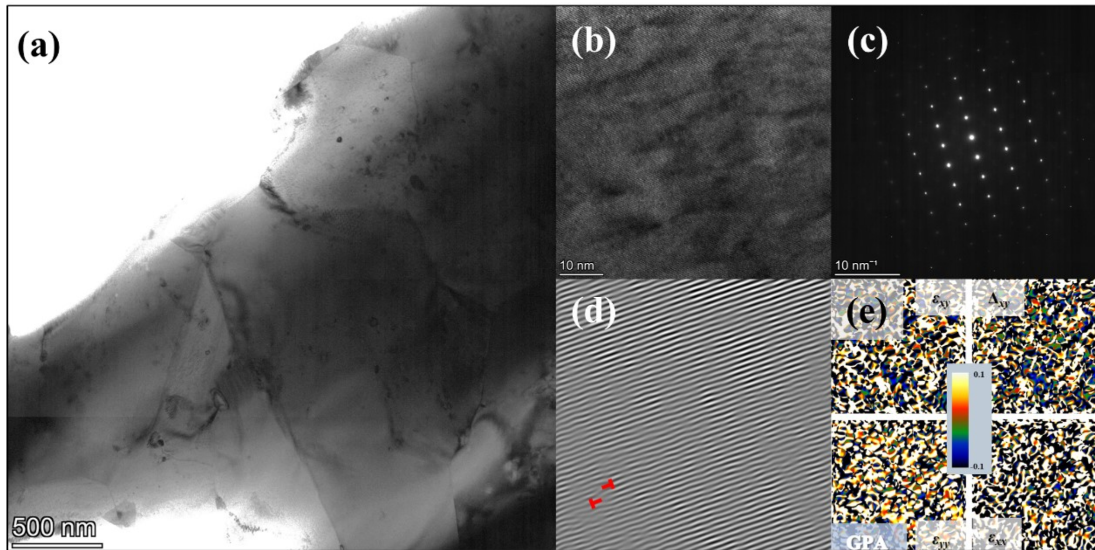

Figure S3. Analysis of microscopic morphology of undoped sample by TEM. (a) Low-resolution and (b) high-resolution TEM images of $Bi_{0.4}Sb_{1.6}Te_3$ matrix. (c) The electron diffraction pattern for (b). (d) The inverse fast Fourier transformation image and (e) the geometric phase analysis image for (b) to indicate the dislocations and stress–strain distribution.

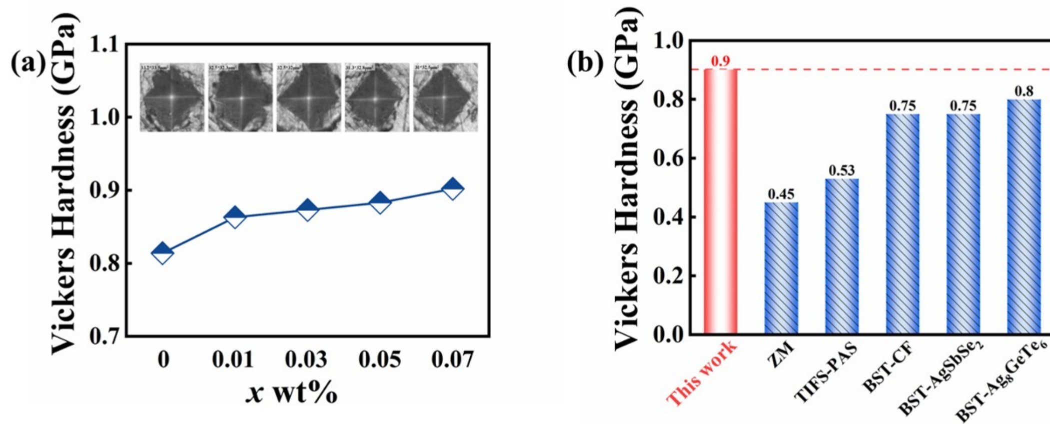

Figure S4. The characterization of Vickers microhardness. (a) The Vickers microhardness of Ag_9GaTe_6-doped $Bi_{0.4}Sb_{1.6}Te_3$ samples and (b) some literature data are shown for comparison.[1-4]

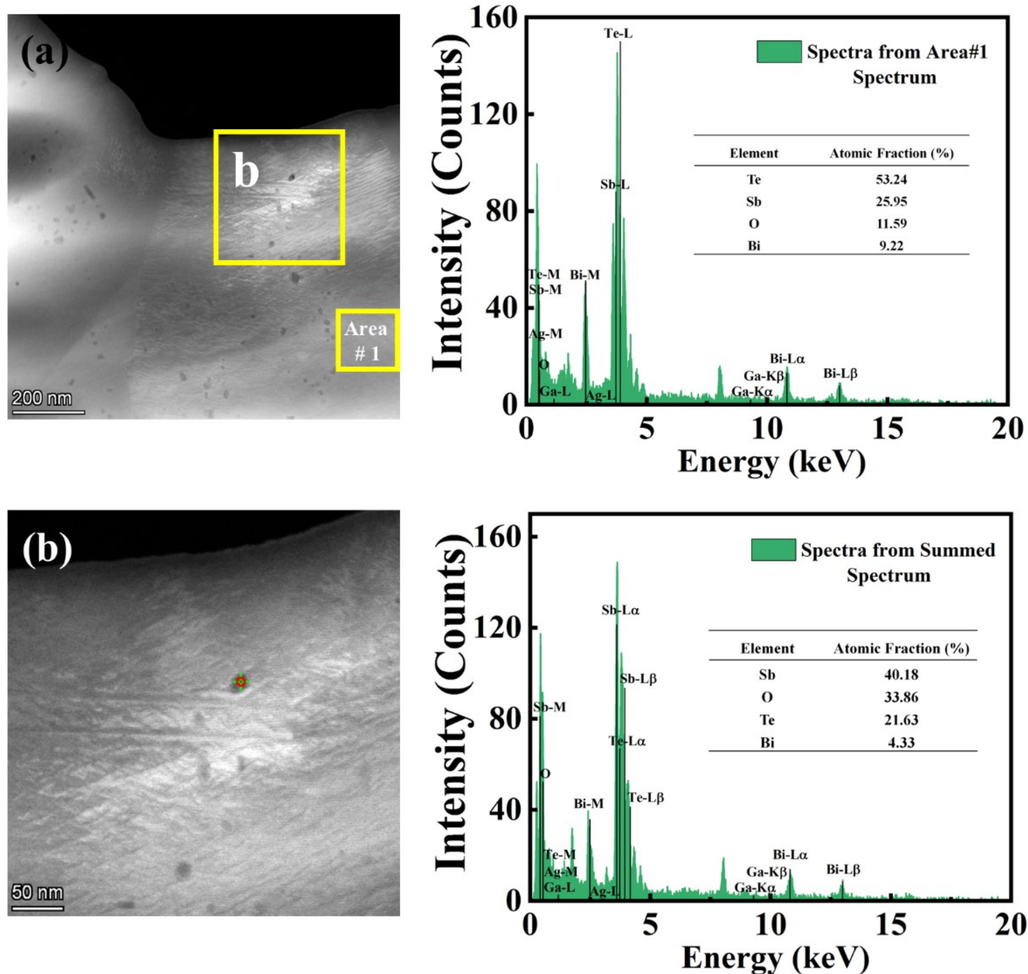

Figure S5. High-angle annular dark-field (HAADF) image without impurity to get the actual atomic fraction of $Bi_{0.4}Sb_{1.6}Te_3$ + 0.03 wt% Ag_9GaTe_6, blank area#1in (a) and nano-particles of (b).

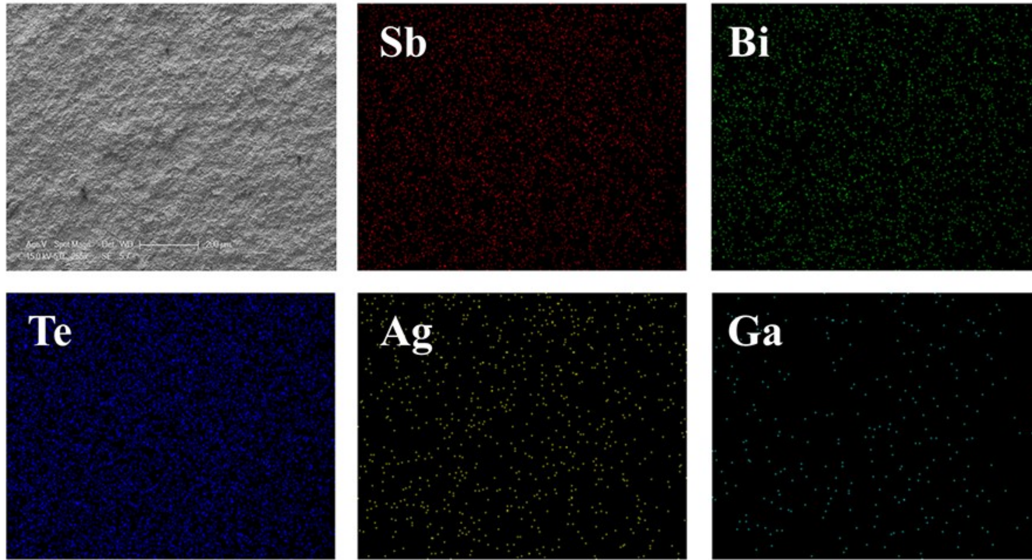

Figure S6. The $Bi_{0.4}Sb_{1.6}Te_3$ + 0.03 wt% Ag_9GaTe_6 sample's EDS elemental mapping of Bi, Sb, Te, Ag and Ga elements.

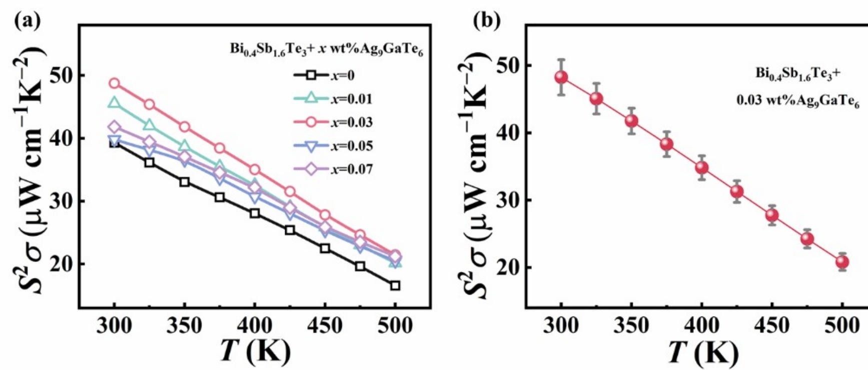

Figure S7. Temperature dependence of power factor for $Bi_{0.4}Sb_{1.6}Te_3$+ x wt% Ag_9GaTe_6 samples.

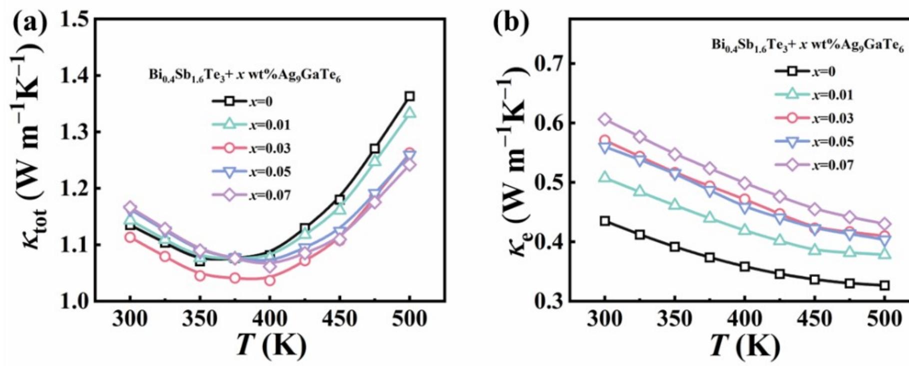

Figure S8. Temperature dependence of a) total thermal conductivity and b) electronic thermal conductivity for $Bi_{0.4}Sb_{1.6}Te_3$+ *x* wt% Ag_9GaTe_6 samples.

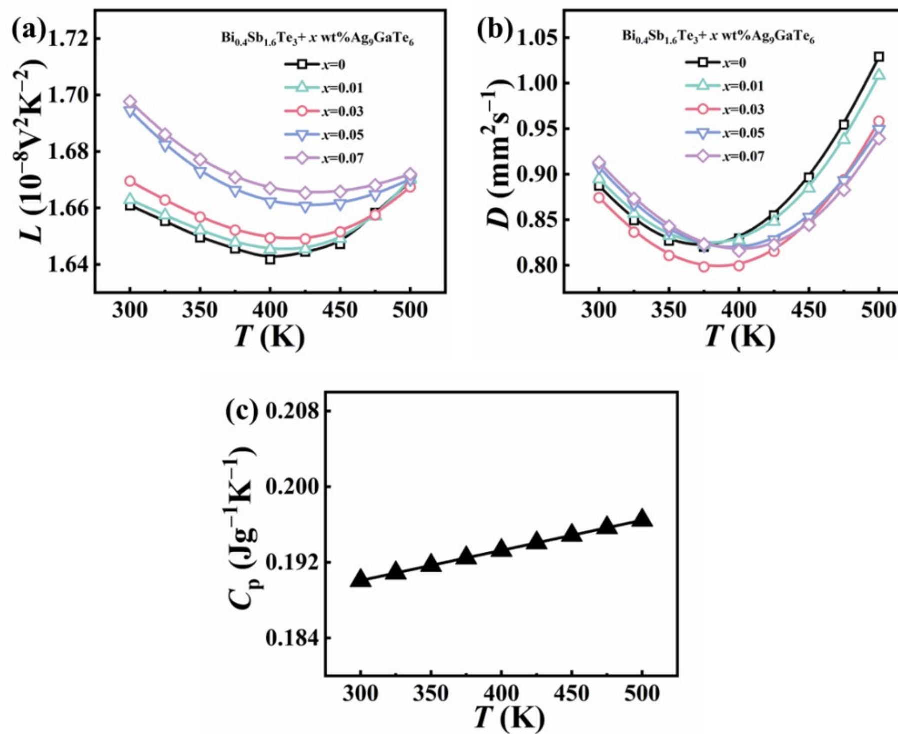

Figure S9. The measured (a) calculated Lorenz number *L*, (b) thermal diffusivity *D*, and (c) the heat capacity C_p of the $Bi_{0.4}Sb_{1.6}Te_3$+ *x* wt% Ag_9GaTe_6 samples.

Table S1. The measured density ρ for the $Bi_{0.4}Sb_{1.6}Te_3$+ x wt% Ag_9GaTe_6 samples.

x	0	0.01	0.03	0.05	0.07
ρ (g cm^{-3})	6.742	6.7415	6.714	6.746	6.731

Debye-Callaway model

The contribution of different defects to lattice thermal conductivity of the $Bi_{0.4}Sb_{1.6}Te_3$+ x wt% Ag_9GaTe_6 can be further explained by Debye-Callaway model. And the lattice thermal conductivity κ_l can be expressed as follows.[5, 6]

$$\kappa_l = \frac{k_B}{2\pi^2 v}\left(\frac{k_B T}{\hbar}\right)^3 \int_0^{\Theta_D/T} \tau_{tot}(x) x^4 e^x ex - 12dx$$

The spectral lattice thermal conductivity (κ_s) is in the integrand term.

$$\kappa_s = \frac{k_B}{2\pi^2 v}\left(\frac{k_B T}{\hbar}\right)^3 \frac{x^4 e^x}{\tau_{tot}^{-1}(x)\left(e^x - 1\right)^2}$$

In the expression, k_B is the Boltzmann constant, v is the in-plane average velocity of phonon, $\hbar$ is the reduced Plank constant, $x = h\omega/k_B T$ (ω indicates the phonon frequency) is the reduced phonon frequency , ϑ_D is the Debye temperature, and τ_{tot} is the total phonon scattering relaxation time, which can be obtained according to the Matthiessen rule, including phonon-phonon Umklapp scattering (U), grain boundary scattering (B), point defect scattering (PD), and dislocation scattering (D) consisting of dislocation strain scattering (DS) and dislocation cores scattering (DC).

$$\tau_{tot}^{-1} = \tau_U^{-1} + \tau_{PD}^{-1} + \tau_{GB}^{-1} + \tau_D^{-1} + \tau_{SP}^{-1}$$

The calculation of the relaxation time related to Umklapp phonon-phonon scattering (τ_U) can be calculated with the following equation.

$$\tau_U^{-1} = A_N \frac{2}{\left(6\pi^2\right)^{1/3}} \frac{k_B V^{1/3} \gamma^2 \omega^2 T}{M v^3}$$

A_N is the pre-factor of Umklapp scattering time, which can be obtained by fitting in-plane transport parameters of the ZM sample. V, γ, and M are the average atomic volume, Grüneisen parameter, and the average atomic mass, respectively.

The relaxation time associated with grain boundary phonon scattering (τ_B) is calculated from:

$$\tau_B^{-1} = \frac{v}{d}$$

in which v is in-plane average speed of sound and d is the average grain size.

The grain boundary phonon scattering (τ_{PD}^{-1}) is estimated by:

$$\tau_{PD}^{-1} = \frac{V\omega^4}{4\pi v^3}\Gamma$$

in which Γ is point defect scattering parameter and the expression is as follows.

$$\Gamma = x(1-x)\left[\left(\frac{\Delta M}{M}\right)^2 + \frac{2}{9}\left\{(G+6.4\gamma)\frac{1+r}{1-r}\right\}^2\left(\frac{\Delta a}{a}\right)^2\right]$$

in which *x* is the fractional concentration of either of constituents. *ΔM, G, r*, and *Δa* are difference in mass, parameter representing a ratio of fractional change of bulk modulus to that of local bond length, Poisson's ratio, and the difference in lattice constant, respectively.

The dislocation strain scattering (τ_{DS}^{-1}) and dislocation cores scattering τ_{DC}^{-1} are calculated by:

$$\tau_{\mathrm{DS}}^{-1} = 0.6B_{\mathrm{D}}^2 N_{\mathrm{D}}(\gamma + \Delta\gamma)^2 \omega \left\{\frac{1}{2} + \frac{1}{24}\left(\frac{1-2r}{1-r}\right)^2\left[1+\sqrt{2}\left(\frac{\upsilon_{\mathrm{L}}}{\upsilon_{\mathrm{T}}}\right)\right]^2\right\} + N_{\mathrm{D}}\frac{V^{4/3}}{v^2}\omega^3$$

in which N_{D}, B_{D}, γ, $\Delta\gamma$, υ_{L}, υ_{T} are dislocation density, effective Burger's vector, Grüneisen parameter, change in Grüneisen parameter, longitudinal phonon velocity, and transverse phonon velocity, respectively.

$$\gamma = \gamma_{\mathrm{pure}} + \gamma_1$$

$$\gamma_1 = \frac{V_{\mathrm{Sb_2Te_3}} C_0 K}{k_{\mathrm{B}} T_{\mathrm{a}}}(\gamma_{\mathrm{pure}}\alpha^2 - \alpha\beta)$$

$$\alpha = \frac{V_{\mathrm{Bi_2Te_3}} - V_{\mathrm{Sb_2Te_3}}}{V_{\mathrm{Sb_2Te_3}}}$$

$$\beta = \frac{M_{\mathrm{Sb_2Te_3}} - M_{\mathrm{Bi_2Te_3}}}{2M_{\mathrm{Bi_2Te_3}}}$$

in which B_D, N_D, C_0, K, T_a, γ_{pure} and γ_1 is the Burger's vector, the dislocation density, the concentration of Bi_2Te_3 in $Bi_{0.4}Sb_{1.6}Te_3$, the bulk modulus of Bi_2Te_3, the sintering temperature, the Grüneisen parameter and the change in Grüneisen parameter, respectively.

Table S2. Parameters for the lattice thermal conductivity of Bi_2Te_3-based materials in the Debye-Callaway model.

Parameters	Description	Values	Ref
ϑ_D	Debye temperature	94K	5
B_D	Effective Burger's vector	1.2×10-9m	fitted
v_L	Longitudinal phonon velocity	2884m s^{-1}	7
v_T	Transverse phonon velocity	1780m s^{-1}	8
v	In-plane average velocity of phonon	2147m s^{-1}	8
γ	Grüneisen parameter	2.33	8
r	Poisson's ratio	0.24	9
V	Average atomic volume of $Bi_{0.4}Sb_{1.6}Te_3$	31.26Å^3	9
V_{BT}	Atomic volume of Bi_2Te_3	3.40×10-29m^3	
V_{ST}	Atomic volume of Sb_2Te_3	3.31×10-29m^3	
M_{BT}	Atomic mass of Bi_2Te_3	2.79×10-25kg	
M_{ST}	Atomic mass of Sb_2Te_3	2.07×10-25kg	
C_0	Concentration of $Bi_{0.4}Sb_{1.6}Te_3$ in Bi_2Te_3	0.2	
K	Bulk modulus	44.8GPa	8
T_a	Sample Sintering temperature	693K	Exp.

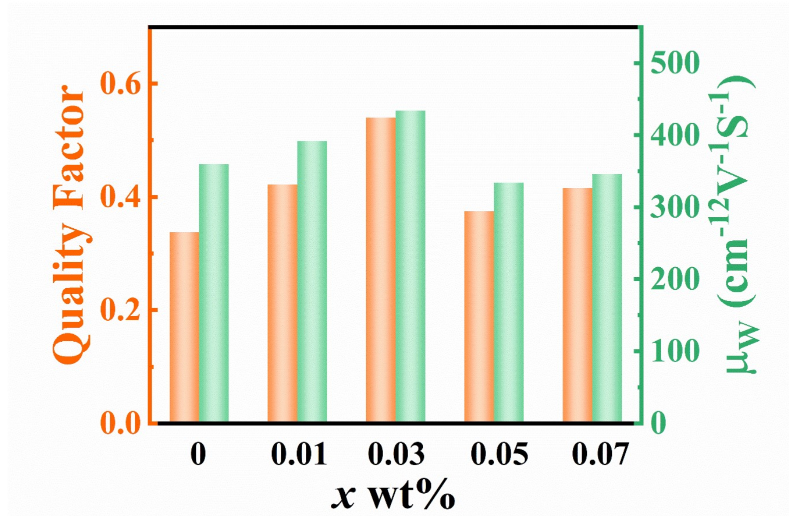

Figure S10. The variation of quality factor B and weighed mobility μ_W of representative samples at room temperature.

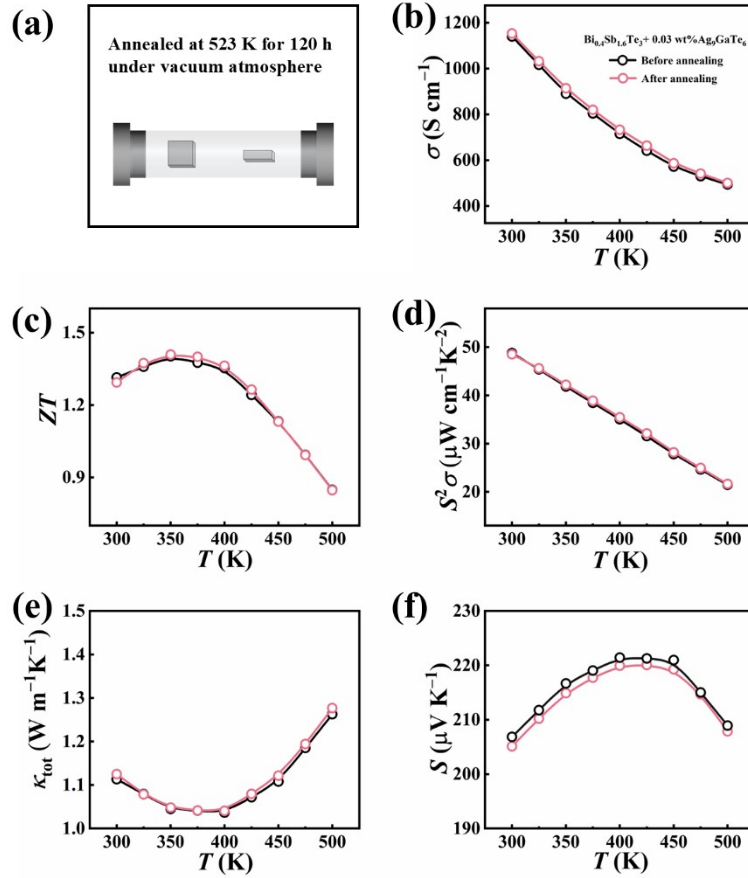

Figure S11. The anneal test of the $Bi_{0.4}Sb_{1.6}Te_3$ + 0.03 wt% Ag_9GaTe_6 sample at 523 K for 120 h under vacuum atmosphere.

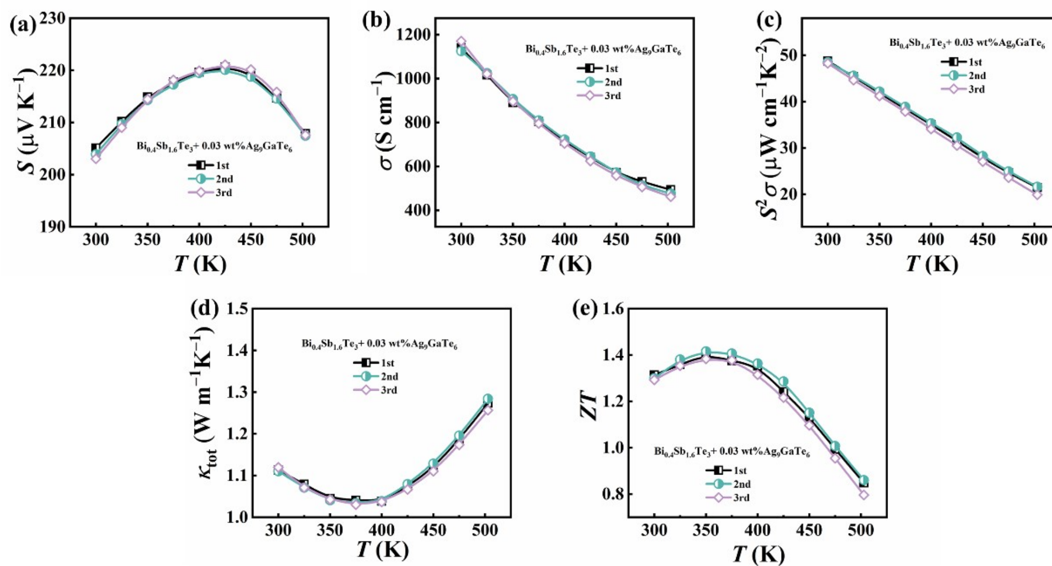

Figure S12. The repeatability test for thermoelectric performance of the $Bi_{0.4}Sb_{1.6}Te_3$ + 0.03 wt% Ag_9GaTe_6 sample.

Statistical analysis for materials:

The electronic and thermal transport parameters were measured by using the commercial ZEM-3 and LFA-457 instruments, respectively. The measured results hardly depend on the sample size, and the errors are mainly the standard deviations of these instruments. Specifically, the systematic errors of Seebeck coefficient S and electrical conductivity σ measurements are about 3% and 5%, respectively. The combined uncertainty for the total thermal conductivity κ_{tot} is about 7% calculated from $\frac{d\kappa tot}{\kappa tot} = \sqrt{(\frac{d\rho}{\rho})^2 + (\frac{dC_p}{C_p})^2 + (\frac{dD}{D})^2}$. 1% for the density ρ, 5% for the specific heat Cp, and 5% for the thermal diffusion D. Ultimately, the uncertainty of the ZT value is estimated to be about 10%. The computational formula involved is $\frac{d(ZT)}{ZT} = \sqrt{(2 \times \frac{dS}{s})^2 + (\frac{d\sigma}{\sigma})^2 + (\frac{d\kappa tot}{\kappa tot})^2}$.

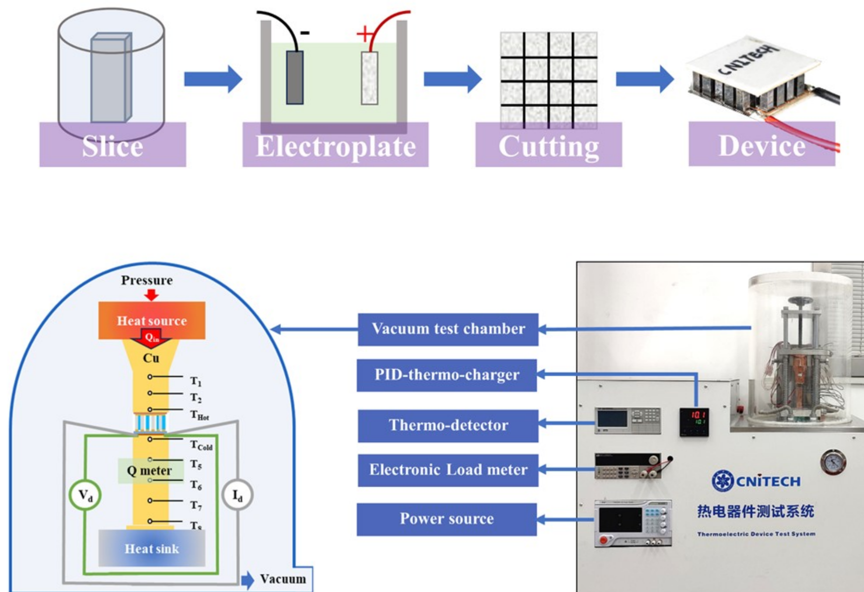

Figure S12. The flowchart of thermoelectric module preparation and the home-built testing system for the thermoelectric module conversion efficiency η measurement.

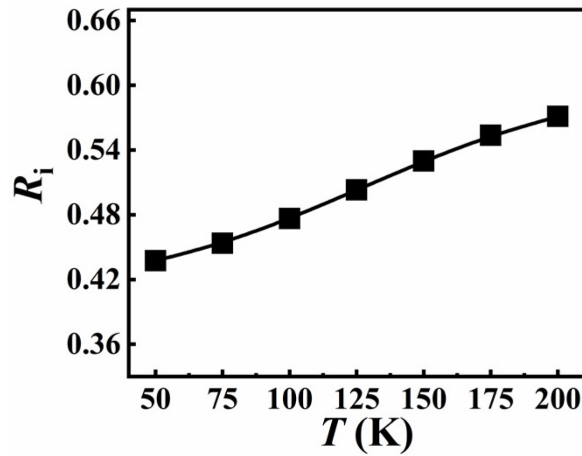

Figure S13. The internal resistance of the $Bi_{0.4}Sb_{1.6}Te_3$ + 0.03wt% Ag_9GaTe_6 sample.

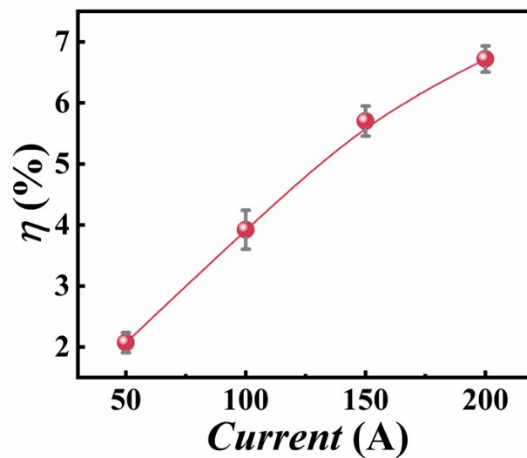

Figure S14. The conversion efficiency of remade Bi_2Te_3-based TE modules in the circuit.

Statistical analysis for modules:

The uncertainty in conversion efficiency is approximately 6%. The measurement error associated with conversion efficiency using the home-built instrument can be analyzed through standard error analysis and propagation methods. Specifically, the uncertainty in thermal conductivity measurements for copper is 5%, while the uncertainties for A_{Cu}, l_{Cu}, I, U and T are 0.5%, 1.5%, 0.5%, 0.5%, and ±0.1%, respectively. The uncertainty is calculated using the following equations:

$$\delta(\Delta T_{Cu}) = \sqrt{[T_{Cu1} \times \delta(T_{Cu1})]^2 + [T_{Cu2} \times \delta(T_{Cu2})]^2}/(T_{Cu1} - T_{Cu2})$$

$$\delta(Q) = \sqrt{\delta(\Delta T_{Cu})^2 + \delta(\kappa_{Cu})^2 + \delta(A_{Cu})^2 + \delta(l_{Cu})^2}$$

$$\delta(P) = \sqrt{\delta(I)^2 + \delta(U)^2}$$

$$\delta(P+Q) = \sqrt{[P \times \delta(P)]^2 + [Q \times \delta(Q)]^2}/(P+Q)$$

$$\delta(\eta) = \sqrt{\delta(P)^2 + \delta(P+Q)^2}$$

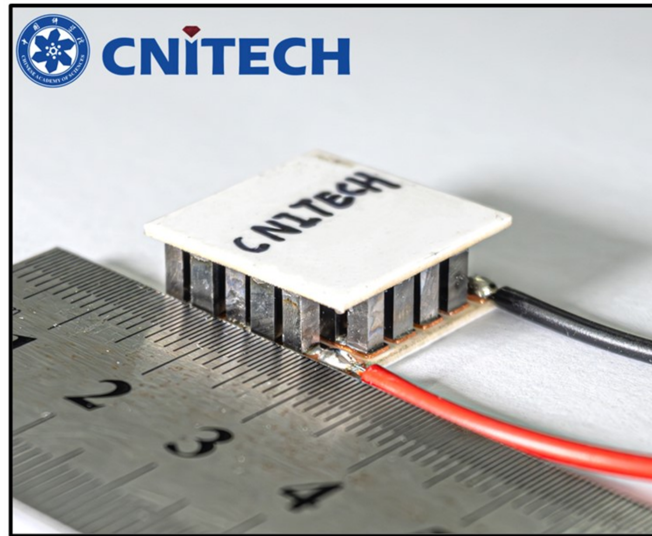

Figure S15. Optical images of the fabricated TE module composed of the *p*-type $Bi_{0.4}Sb_{1.6}Te_3$ + 0.03 wt% Ag_9GaTe_6 and zone-melted n-type $Bi_2Te_{2.7}S_{e0.3}$.

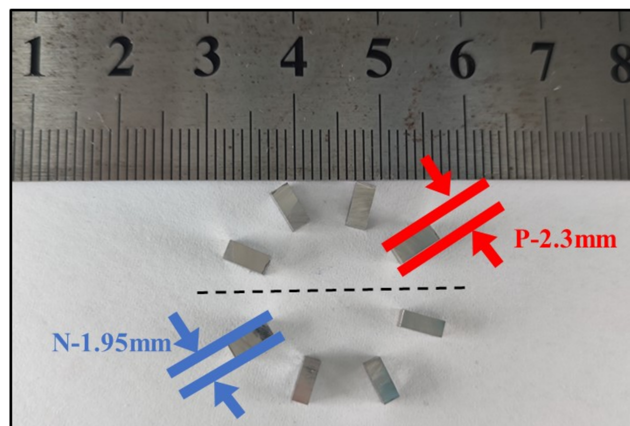

Figure S16. Comparison of geometric dimensions of the *n*/ *p* type TE legs.

Table S3. The thermoelectric behaviors of *n*-type $Bi_2Te_{2.7}Se_{0.3}$ zone-melted materials in the thermoelectric modules.

T (K)	σ (S cm^{-1})	S (μV K^{-1})	κ_{tot} (W m^{-1} K^{-1})
300	1326	-201	1.56
350	1116	-211	1.53
400	948	-214	1.65
450	845	-204	1.95
500	807	-182	2.38

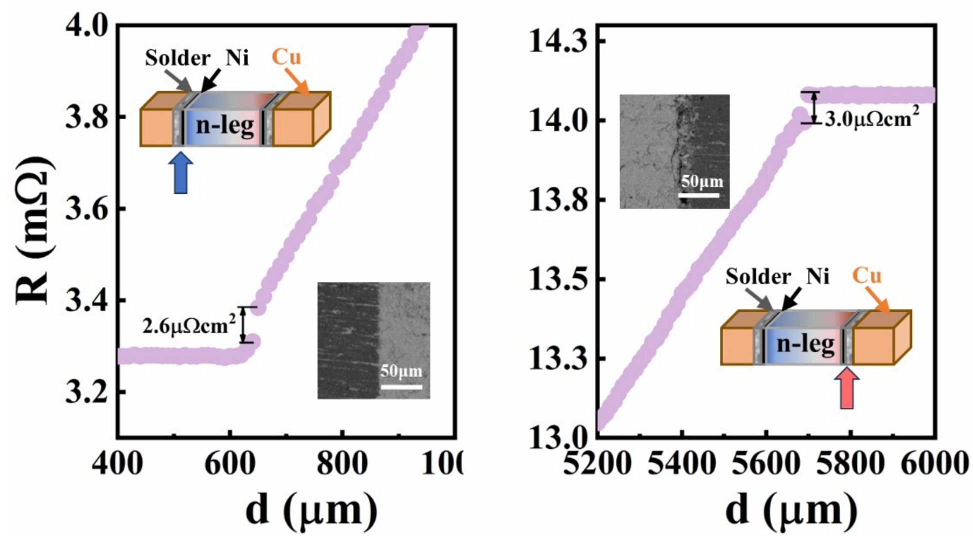

Figure S17. The measured contact resistance by the scanning of resistance across the Cu-Bi2Te3 interfaces for n-leg, with the inset of SEM images.

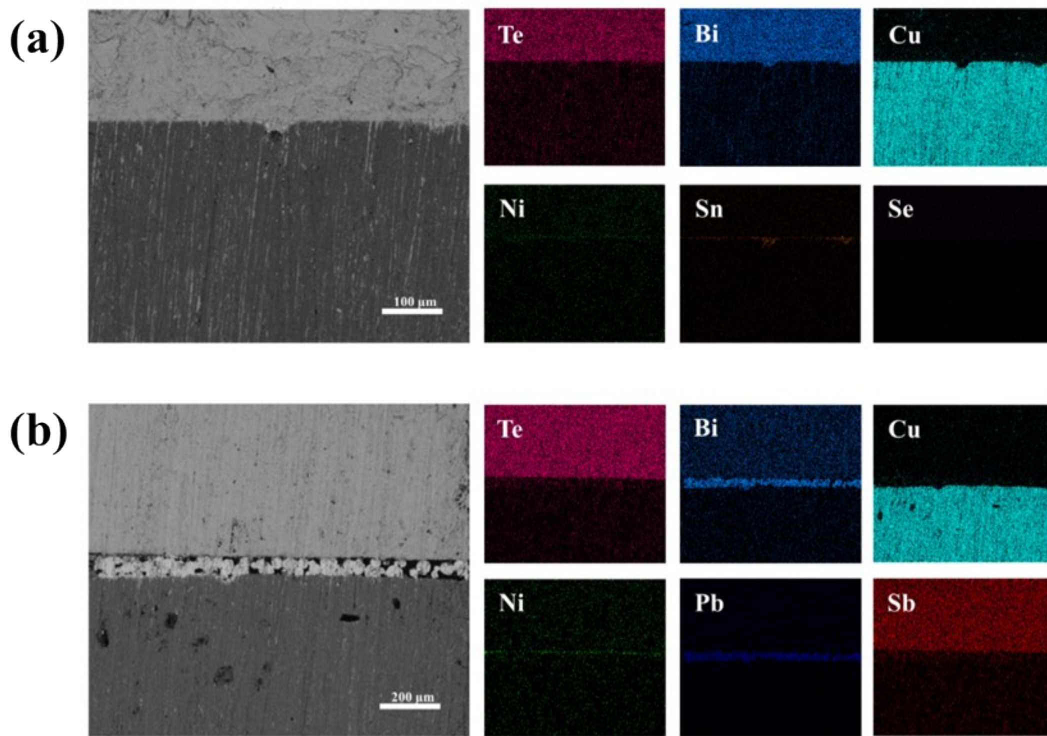

Figure S18. The SEM image and EDS mapping of the interface between Cu electrode and *p*-leg (a) cold-side, (b) hot-side.

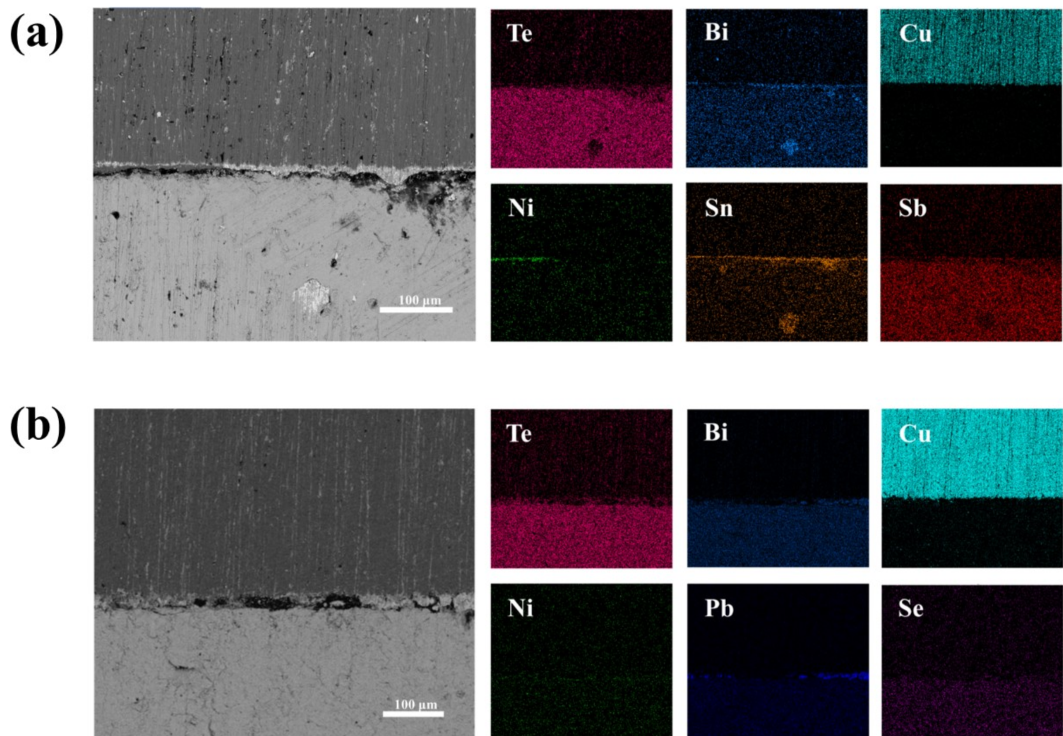

Figure S19. The SEM image and EDS mapping of the interface between Cu electrode and *n*-leg (a) cold-side, (b) hot-side.

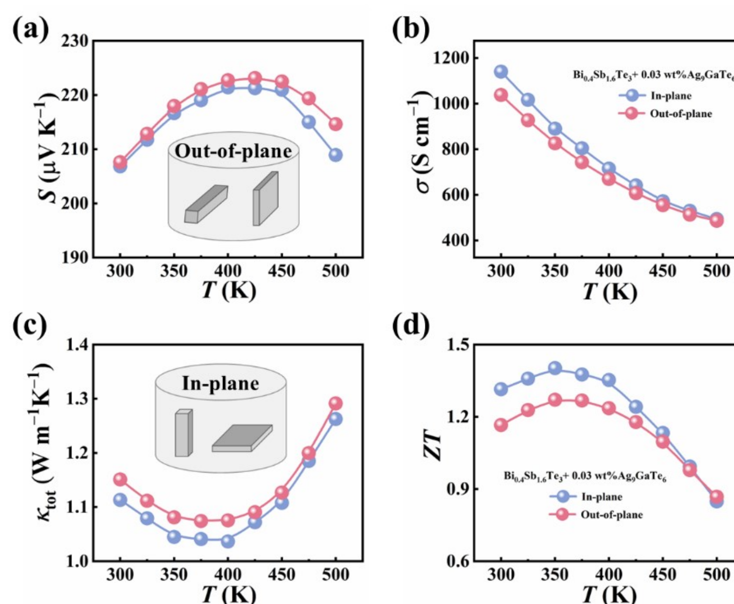

Figure S19. Comparison of electronic and thermal transport properties of the representative $Bi_{0.4}Sb_{1.6}Te_3$ + 0.03 wt% Ag_9GaTe_6 sample in both·the out-of-plane" and·in-plane directions, including a) Seebeck coefficient, b)electrical conductivity, c)total thermal conductivity, and d) ZT value.

The synthesis method of Ag_9GaTe_6

The Ag_9GaTe_6 polycrystalline samples were prepared from appropriate amounts of Ag (4N), Ga(4N), Te(4N) elements. The mixture was melted in sealed quartz ampoules at 1243 K for 6 h and annealed at 893 K for 72 h, and then made into fine powder by ball milling.

References

1. R. Deng, X. Su, S. Hao, Z. Zheng, M. Zhang, H. Xie, W. Liu, Y. Yan, C. Wolverton, C. Uher, M. G. Kanatzidis and X. Tang, *Energy Environ. Sci.*, 2018, **11**, 1520-1535.
2. Q. Zhang, G. Wu, Z. Guo, P. Sun, R. Wang, L. Chen, X. Wang, X. Tan, H. Hu, B. Yu, J. G. Noudem, G. Liu and J. Jiang, *ACS Appl. Mater. Interfaces*, 2021, **13**, 24937-24944.
3. Q. Zhang, M. Yuan, K. Pang, Y. Zhang, R. Wang, X. Tan, G. Wu, H. Hu, J. Wu, P. Sun, G. Q. Liu and J. Jiang, *Adv. Mater.*, 2023, **35**, 2300338.
4. G. Yang, L. Sang, F. F. Yun, D. R. G. Mitchell, G. Casillas, N. Ye, K. See, J. Pei, X. Wang, J. F. Li, G. J. Snyder and X. Wang, *Adv. Funct. Mater.*, 2021, **31**, 2008851.
5. D. Bessas, I. Sergueev, H. C. Wille, J. Perßon, D. Ebling and R. P. Hermann, *Physical Review B*, 2012, **86**, 224301.
6. J. Callaway and H. C. von Baeyer, *Physical Review*, 1960, **120**, 1149-1154.
7. F. Yang, T. Ikeda, G. J. Snyder and C. Dames, *J. Appl. Phys.*, 2010, **108**, 034310.
8. X. Chen, H. D. Zhou, A. Kiswandhi, I. Miotkowski, Y. P. Chen, P. A. Sharma, A. L. Lima Sharma, M. A. Hekmaty, D. Smirnov and Z. Jiang, *Appl. Phys. Lett.*, 2011, **99**, 261912.
9. E. S. Toberer, A. Zevalkink and G. J. Snyder, *J. Mater. Chem.*, 2011, **21**, 15843-15852.